JGR Space Physics

RESEARCH ARTICLE
10.1029/2022JA030686

Key Points:

- We study the helicity sign of Flux Transfer Events and investigate upstream solar wind conditions and local magnetic shear around them
- The helicity sign is found to be unassociated to the Interplanetary Magnetic Field (B_y) component when the local magnetic shear is high
- The FTEs' helicity sign in such cases may relate to the Hall field of magnetic reconnection in the absence of a guide field

Supporting Information:

Supporting Information may be found in the online version of this article.

Correspondence to:

S. Dahani,
sdahani@irap.omp.eu

Citation:

Dahani, S., Kieokaew, R., Génot, V., Lavraud, B., Chen, Y., Michotte de Welle, B., et al. (2022). The helicity sign of flux transfer event flux ropes and its relationship to the guide field and hall physics in magnetic reconnection at the magnetopause. *Journal of Geophysical Research: Space Physics*, *127*, e2022JA030686. https://doi.org/10.1029/2022JA030686

Received 27 MAY 2022
Accepted 22 OCT 2022

The Helicity Sign of Flux Transfer Event Flux Ropes and Its Relationship to the Guide Field and Hall Physics in Magnetic Reconnection at the Magnetopause

S. Dahani[1], R. Kieokaew[1], V. Génot[1], B. Lavraud[1,2], Y. Chen[3], B. Michotte de Welle[4], N. Aunai[4], G. Tóth[5], P. A. Cassak[6], N. Fargette[1], R. C. Fear[7], A. Marchaudon[1], D. Gershman[8], B. Giles[8], R. Torbert[9], and J. Burch[10]

[1]Institut de Recherche en Astrophysique et Planétologie, CNRS, UPS, CNES, Université de Toulouse, Toulouse, France, [2]Laboratoire d'Astrophysique de Bordeaux, CNRS, University of Bordeaux, Pessac, France, [3]Department of Astrophysical Sciences and Princeton Plasma Physics Laboratory, Princeton University, Princeton, NJ, USA, [4]CNRS, UPMC, Laboratory of Plasma Physics, Ecole Polytechnique, Université Paris Sud, Orsay, France, [5]Department of Climate and Space Sciences and Engineering, University of Michigan, Ann Arbor, MI, USA, [6]Department of Physics and Astronomy and center for KINETIC Plasma Physics, West Virginia University, Morgantown, WV, USA, [7]School of Physics, Astronomy, University of Southampton, Southampton, UK, [8]NASA Goddard Space Flight Center, Greenbelt, MD, USA, [9]Space Science Center, University of New Hampshire, Durham, NH, USA, [10]Southwest Research Institute, San Antonio, TX, USA

Abstract Flux Transfer Events (FTEs) are transient magnetic flux ropes typically found at the Earth's magnetopause on the dayside. While it is known that FTEs are generated by magnetic reconnection, it remains unclear how the details of magnetic reconnection controls their properties. A recent study showed that the helicity sign of FTEs positively correlates with the east-west (B_y) component of the Interplanetary Magnetic Field (IMF). With data from the Cluster and Magnetospheric Multiscale missions, we performed a statistical study of 166 quasi force-free FTEs. We focus on their helicity sign and possible association with upstream solar wind conditions and local magnetic reconnection properties. Using both in situ data and magnetic shear modeling, we find that FTEs whose helicity sign corresponds to the IMF B_y are associated with moderate magnetic shears while those that do not correspond to the IMF B_y are associated with higher magnetic shears. While uncertainty in IMF propagation to the magnetopause may lead to randomness in the determination of the flux rope core field and helicity, we rather propose that for small IMF B_y, which corresponds to high shear and low guide field, the Hall pattern of magnetic reconnection determines the FTE core field and helicity sign. In that context we explain how the temporal sequence of multiple X-line formation and the reconnection rate are important in determining the flux rope helicity sign. This work highlights a fundamental connection between kinetic processes at work in magnetic reconnection and the macroscale structure of FTEs.

Plain Language Summary In the vicinity of the Earth's magnetosphere outer boundary, the magnetopause, twisted magnetic field structures known as "Flux Transfer Events" (FTEs) are often detected by spacecraft in-situ. They temporarily connect the solar wind to the Earth's ionosphere, allowing the transfer of solar wind flux into the magnetosphere. It is known that FTEs are produced as a consequence of magnetic reconnection, a process that rearranges the topology of sheared magnetic fields, between the shocked solar wind and the geomagnetic field. However, our understanding of how the microphysics of magnetic reconnection can lead to the macroscopic structures of FTEs is still limited. We revisit the in-situ observations of FTEs made by the Cluster and Magnetospheric Multiscale missions. We focus on the twist feature of FTEs as characterized by their helicity and investigate its relationship to solar wind conditions and possible link to magnetic reconnection properties. By investigating local magnetic shear conditions around FTE locations, we found that the FTE helicity is determined by a kinetic feature of magnetic reconnection known as the "Hall magnetic field". Our study highlights a close connection between a kinetic process of magnetic reconnection and the global structure of FTEs, constituting a cross-scale coupling effect in solar-terrestrial interaction.

1. Introduction

Flux Transfer Events (FTEs) are magnetic flux ropes produced at the dayside magnetopause as a consequence of magnetic reconnection. They were first observed by Russell and Elphic (1978) using magnetic field measurement from ISEE 1 and 2. An FTE is recognised in in-situ spacecraft time-series data as a bipolar variation in the

magnetic field component normal to the magnetopause (i.e., magnetic field B_N). The bipolar signature consists of a variation of the magnetic field from positive to negative or negative to positive as reported by Russell and Elphic (1979) and Rijnbeek et al. (1982). For typical FTEs, the bipolar signature is co-located with an enhancement in the magnetic field strength compared to the ambient field (e.g., Paschmann et al., 1982), although this enhancement may depend on the spacecraft trajectory (e.g., H. Zhang et al., 2010). A less-common type of FTEs, called crater FTEs (e.g., Farrugia et al., 1988; 2011; LaBelle et al., 1987; Sibeck et al., 2008; Trenchi et al., 2019; H. Zhang et al., 2010), has dips at the center of the enhanced magnetic field strength; it was suggested to be a signature of early-stage FTEs (H. Zhang et al., 2010; 2012).

Various mechanisms were suggested to explain the formation of FTEs. Lee and Fu (1985) proposed that an FTE is created between two reconnection X-lines formed simultaneously on the dayside magnetopause. Using global magnetohydrodynamics (MHD) simulations, Raeder (2006) showed that FTEs can be generated by sequential, magnetic reconnection where reconnection X-lines are formed one after the other under a large dipole tilt condition (e.g., during the winter/summer season on the Northern/Southern hemisphere); Dorelli and Bhattacharjee (2009) later showed that the dipole tilt is not required to produce FTEs. Other formation mechanisms were also proposed based on single X-line reconnection due to the nature of unsteady or transient reconnection (e.g., Southwood et al., 1988; Scholer, 1988). More recently, there are increasing evidence supporting FTE generation due to multiple X-line reconnection (e.g., Hasegawa et al., 2010; Kieokaew et al., 2021; Øieroset et al., 2011; Trenchi et al., 2011). After their initial formation, FTEs undergo dynamical evolution due to continuous reconnection while propagating poleward (e.g., Akhavan-Tafti et al., 2019; Hoilijoki et al., 2019; Hwang et al., 2020; Guo et al., 2021). Using a 2-D hybrid-Vlasov simulation, Akhavan-Tafti et al. (2020) demonstrated that magnetic islands (magnetic flux ropes in 3-D) can coalesce, erode, or divide due to reconnection at their periphery during the evolution. Such dynamical processes were believed to lead to FTE growth after their generation. In this study, we mainly focus on the FTE generation by the classical scenarios which involve single and multiple X-line reconnection.

An FTE flux rope has a helical, twisted interior (e.g., Cowley, 1982; Russell & Elphic, 1979; Saunders et al., 1984). Magnetic helicity is an ideal MHD invariant defined as $\mathcal{H} = \int_V \boldsymbol{A} \cdot \boldsymbol{B} dV$, where $\boldsymbol{A}$ is the magnetic vector potential, $\boldsymbol{B}$ is the magnetic field, and V is the integration volume. Magnetic helicity is a useful quantity for characterizing topology of magnetic structures (e.g., Berger & Field, 1984; Berger, 1999; Song & Lysak, 1989; Wright & Berger, 1990). In particular, the sign of magnetic helicity, namely "handedness", or "chirality", has been used to characterize the sense of the twist in the flux rope interior into right-handed ($H = +1$) and left-handed ($H = -1$) (e.g., Bothmer & Schwenn, 1998; Burlaga, 1988; Lepping et al., 1990). Studies of the helicity sign of magnetic flux ropes in various environments such as in interplanetary space (e.g., Bothmer & Schwenn, 1998; Dasso et al., 2003; Leamon et al., 2004; Pal, 2022), planetary magnetospheres (e.g., Martin et al., 2020; Russell, 1990; Wei et al., 2010), and Earth's magnetosphere (e.g., Eastwood et al., 2012; Kieokaew et al., 2021; H. Zhang et al., 2010) have led to a better understanding of their origins. The total magnetic helicity, defined in a volume bounded by perfectly conducting walls, is generally conserved. During magnetic reconnection, the total magnetic helicity remains conserved as well (e.g., Berger, 1982; Berger, 1984), on time scales shorter than the global diffusion time scale. In this study, we do not calculate the full helicity but merely focus on the sign of magnetic helicity as obtained from fitting magnetic field data to a constant-alpha force-free flux rope model (e.g., Burlaga, 1988; Lepping et al., 1990).

Recently, Kieokaew et al. (2021) studied the helicity sign of FTEs and its relationship with the Interplanetary Magnetic Field (IMF). They found that the helicity sign of most FTEs correlates to the IMF B_y polarity, further revealing a close relationship between solar wind conditions and the formation of FTEs. Based on geometrical considerations of FTE formation under southward IMF conditions, they hypothesised that the flux rope twist direction should correspond to the IMF B_y orientation. This hypothesis arose from the configuration of magnetic reconnection in which the IMF B_y component would give a guide field to the reconnecting magnetic field between the draped, southward IMF and the northward geomagnetic field (Lee & Fu, 1985). In the context of FTE generation by multiple X-line reconnection, this guide field (IMF B_y) orientation would directly determine the core field and the helicity sign of the flux rope formed between the two X-lines. Under southward IMF, an FTE formed in between multiple X-line reconnection would have a positive helicity sign if it is formed under IMF $B_y > 0$ (i.e., duskward), while it would have a negative helicity sign if it is formed under IMF $B_y < 0$ (i.e., dawnward). Using data from the Magnetospheric MultiScale (MMS) mission, they performed a statistical study of the helicity sign of FTE flux ropes. They found that the majority of events are consistent with this hypothesis. However, there

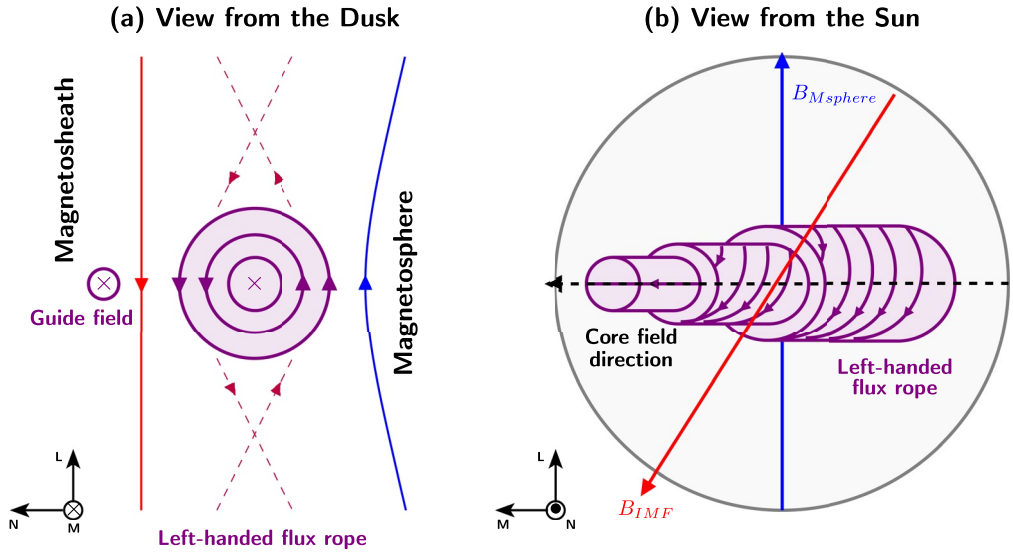

Figure 1. Schematic illustration of FTE formation by multiple X-line reconnection under a significant guide field. This illustration shows a dawnward and southward IMF leading to a dawnward core field and left-handed flux rope. Panel (a) shows a view from the dusk side and panel (b) shows a view from the Sun. The FTE flux rope is represented in purple with arrows indicating the magnetic field direction. Solid blue and red lines represent magnetospheric and magnetosheath field lines, respectively. Adapted from Kieokaew et al. (2021).

were a significant number of events (14 out of 84) that were not consistent with this hypothesis; they called them the outliers, and we will keep this definition in the present work. In other words, in some events, a duskward IMF B_y imposed both a duskward core field and a positive helicity, and in others, a dawnward IMF B_y imposed both a dawnward core field and a negative helicity. Figure 1, adapted from Kieokaew et al. (2021), shows a schematic illustration of a dawnward and southward IMF leading to a dawnkward core field and left-handed flux rope. A duskward and southward IMF would have led to a duskward core field and a right-handed flux rope, highlighting the one-to-one relationship between the core field orientation and the helicity sign that results from guide field reconnection in a scenario where the flux rope is formed by multiple X-lines. In another study, Karimabadi et al. (1999) discussed, based on 2-D and 3-D hybrid simulations, how the core field of flux ropes on the dayside magnetopause and the magnetotail are controlled by the guide field. Teh, Abdullah, and Hasbi (2014) studied the core field of two flux ropes observed at the magnetopause under high magnetic shear. They found that the polarity of the core field of one of the flux ropes is opposite to the guide field produced by reconnection as observed near the flux ropes. In this work, we expand the statistics of Kieokaew et al. (2021) by including FTE observations from the Cluster mission. We investigate in particular the FTE population whose helicity sign is inconsistent with the IMF B_y orientation to understand their formation mechanism.

Here, we investigate the structures of FTEs using the sign of magnetic helicity as a tool to better understand their formation and connection to magnetic reconnection. The outline of this paper is as follows. Section 2 presents data from the Cluster and MMS missions and the methodology for event selection and flux rope fitting. Section 3 presents an example event from MMS and the statistical analyses of all events. Section 4 discusses our findings. Finally, Section 5 presents the conclusions and summary.

2. Data and Methodology

2.1. Data Overview

We utilize data from the Cluster (Escoubet et al., 2001) and MMS (Burch et al., 2016) missions. Cluster made observations at high latitudes ($|Z_{GSE}| > 5\ R_E$), while MMS made observations at low latitudes ($-5\ R_E < Z_{GSE} < 5\ R_E$). We take data from Cluster 1 and Cluster 3. For MMS, we take data only from MMS 1 since all the MMS spacecraft observe identical features across FTE scale size.

For Cluster, we use the FTE list from Fear et al. (2012). The observations were made between November 2002 and June 2003 during the Cluster dayside season. We performed a visual inspection to determine the FTE time interval for each event. The criteria for selection are: (a) clear symmetric and bipolar variation of B_N (the magnetic field component perpendicular to the unperturbed magnetopause), and (b) a clear enhancement in the magnetic field strength. For events observed using MMS, we obtained the list of quasi force-free FTEs from Kieokaew et al. (2021). This list is a subset of the FTE observations using MMS in 2015–2017 (Phases A and B) compiled by Fargette et al. (2020).

We use magnetic field measurements from the Flux Gate Magnetometer (FGM; Balogh et al., 2001) instrument on-board Cluster at 0.2 s resolution in the Geocentric Solar Ecliptic (GSE) coordinate system. Similarly for MMS, we use magnetic field measurements from the FGM instrument on-board MMS (Russell et al., 2016) in both burst and survey modes with resolutions of 0.01 s and 0.06 s, respectively. We use plasma moments consisting of ion bulk flow velocity, ion temperature, and ion number density from the Cluster Ion Spectrometry Hot Ion Analyser (CIS-HIA; Rème et al., 1997) instrument at about 4s resolution on-board Cluster, and the Fast Plasma Investigation (FPI; Pollock et al., 2016) measurements in both burst and survey modes with resolutions of 0.03 s/0.15 s (electrons/ions) and 4.5 s, respectively. Finally, we use solar wind data from the OMNI database (King & Papitashvili, 2005), where the measurements were taken by the Advanced Composition Explorer (ACE) and Wind spacecraft and time-shifted to the bow-shock nose, at 5-min resolution.

2.2. FTE Observation

FTEs in spacecraft time-series data often exhibit clear signatures in the boundary normal coordinate system (LMN) (e.g., Russell & Elphic, 1979). In the LMN system, $\boldsymbol{N}$ is normal to the magnetopause and pointing outward from the Earth, $\boldsymbol{M}$ the cross product of $\boldsymbol{N}$ and the north geomagnetic dipole Z_{GSM} direction ($\boldsymbol{M} = \boldsymbol{N} \times \boldsymbol{Z}_{GSM}$), $\boldsymbol{L}$ completes the right-handed orthonormal system. We adopt the magnetopause model from Shue et al. (1998) for locating the normal direction of the unperturbed magnetopause boundary. The Shue model describes the shape, size and location of the magnetopause boundary based on the function $r = r_0\left(\frac{2}{1+\cos\theta}\right)^{\alpha_{MP}}$, where r_0 is the stand-off distance of the magnetopause from the Earth, α_{MP} is the level of tail flaring, θ is the angle between the r_0 and r directions. r_0 and α_{MP} are empirical functions of the IMF B_z and the solar wind dynamic pressure (P_{dyn}), given as $r_0 = [10.22 + 1.29 \times \tanh(0.184 \times (B_z + 8.14))] \times P_{dyn}^{-1/6.6}$ and $\alpha_{MP} = (0.58 - 0.007 \times B_z) \times (1 + 0.024 \times \ln(P_{dyn}))$.

2.3. Flux Rope Fitting

To obtain the helicity sign of FTE flux ropes, we fit the data to a force-free model derived by Burlaga (1988), which was originally introduced to describe the magnetic field structure of magnetic clouds in the solar wind. The model is a solution of the cylindrically symmetric force-free configuration satisfying the equation $\nabla \times \boldsymbol{B} = \alpha \boldsymbol{B}$, where $\boldsymbol{B}$ is the magnetic field and α is a constant, found by Lundquist (1950). The solution is found to be: $B_A = B_0 J_0(\alpha R)$ for the axial component, $B_T = B_0 H J_1(\alpha R)$ for the tangential component and $B_R = 0$ for the radial component, where $H = \pm 1$ is the helicity sign, R is the radial distance from the axis, J_0 and J_1 are the zeroth and first order Bessel functions of first kind, respectively, and B_0 is the maximum magnetic field strength inside the flux rope.

As introduced in Burlaga (1988), the model fitting is done in a local flux rope frame ($\boldsymbol{x}_v$, $\boldsymbol{y}_v$, $\boldsymbol{z}_v$) (see Figure S1 of Kieokaew et al. (2021), adapted from Figure 2 of Burlaga (1988)). We use a more adapted frame similar to that used in Lepping et al. (1990). We take $\boldsymbol{x}_v$ to be along the direction opposite to the flux rope motion such that $\boldsymbol{x}_v = -\boldsymbol{V}_{av}/|\boldsymbol{V}_{av}|$, where $\boldsymbol{V}_{av}$ is the average flow velocity across the flux rope. We define $\boldsymbol{z}_v = \boldsymbol{n}$, where $\boldsymbol{n}$ is the normal to the model magnetopause and $\boldsymbol{y}_v$ completes the right-handed orthonormal system, i.e., $\boldsymbol{y}_v = \boldsymbol{z}_v \times \boldsymbol{x}_v$. The five parameters describing the flux rope configuration in a local flux rope frame ($\boldsymbol{x}_v$, $\boldsymbol{y}_v$, $\boldsymbol{z}_v$) are: (a) $\theta_0 \in [-90°, 90°]$ the angle between the flux rope axis and the ecliptic plane, (b) $\phi_0 \in [0°, 180°]$ the angle between the axial direction of the flux rope projected on the ecliptic plane and $\boldsymbol{x}_v$, (c) b_0 the distance between the spacecraft and the flux rope motion plane, (d) t_0 the time that corresponds to the closest approach of the flux rope to the spacecraft and (e) α is a constant. The helicity sign H is determined from magnetic field data. Nevertheless, we confirm the helicity sign based on the quality of the resulting fit. As not all flux ropes can be assumed force-free, the

quality of the fit is not always good. Here we select only flux ropes that can be fitted well to the model (i.e., quasi force-free), and for which there is no ambiguity on the helicity sign. We select 82 events from Cluster and 84 from MMS. Table S1 of the Supporting Information for this work lists the 82 events from Cluster with their respective start and end times, their locations in the GSE system and their helicity signs. The MMS events may be found in Table S1 of Kieokaew et al. (2021).

3. Event Illustration and Statistical Analyses

3.1. Event Overview

Figure 2 shows an example of an FTE, detected by MMS1 on November 5th, 2015, between 14:07:07 and 14:07:44 UT. It shows a 10-min interval (top) and a zoom-in (1-min interval; bottom). Panels (a) and (a') present the magnetic field in the GSE coordinate system and its magnitude $|\boldsymbol{B}|$. Panel (b') presents the components of the magnetic field in the ($\boldsymbol{x}_v$, $\boldsymbol{y}_v$, $\boldsymbol{z}_v$) frame. Panel (b) shows the components of the ion velocity in the GSE coordinate system. Panel (c) displays the ion number density. Panel (d) shows the ion temperature in the direction parallel and perpendicular to the magnetic field. Panel (e) presents the ion energy spectrogram. The bipolar signature of the flux rope is visible in panels (a) as shaded in gray, but it is most clearly seen in panel (b') where the B_{zv} component rotates from negative to positive. We also observe an enhancement in the magnetic field strength in panel (a) and (a') during this bipolar variation. In addition, we also observe a slight increase in the temperature in panel (d) during the flux rope interval. The dashed lines in panel (b') represent the flux rope model fit during the flux rope time interval. In this case, the better fit was found for $H = -1$. Therefore, this flux rope twist is categorized as left-handed (LH). To understand the local conditions surrounding this flux rope, we also characterize the adjacent magnetospheric and magnetosheath regions as follows. The region highlighted in red in panels (a) to (e) shows the magnetosphere region adjacent to the flux rope, which is marked between 14:13:45 and 14:14:00 UT. This region is identified by an almost instantaneous drop in the ion number density seen in panel (c) co-located with a dropout in the fluxes of low energy (<1 keV) ions, and with intense fluxes of higher energy ions (>1 keV) that is distinct from the surrounding regions. The region highlighted in green shows the magnetosheath region most adjacent to the flux rope, between 14:06:40 and 14:06:55 UT. This region is identified with the larger density and lower temperature.

3.2. Spatial Distribution

Figure 3 shows the spatial distribution of all the events in the GSE coordinate system. Crosses represent RH ($H = +1$) flux ropes and triangles represents LH ($H = -1$) flux ropes. Panel (a) shows a projection in the $Y_{GSE} - Z_{GSE}$ plane as viewed from the Sun (positive X_{GSE}), and panel (b) is a projection in the $X_{GSE} - Y_{GSE}$ plane as viewed from the north (positive Z_{GSE}), with the approximate magnetopause boundary using the average IMF B_z and P_{dyn} from the Shue model. The MMS events are located in the low latitude region, while Cluster events are located at higher latitudes and further from the nose. There are more events on the dusk side (positive Y_{GSE}) than on the dawn side. From our investigation, these events are often found downstream of quasi-perpendicular shocks, where the magnetosheath data are often more laminar (which lead to an easier identification of FTEs). Nevertheless, there is no spatial preferences for the RH and LH flux ropes as they appear to be distributed almost uniformly across the planes.

3.3. Solar Wind Conditions

To revisit the correlation between the IMF B_y and the FTE helcity sign, we analyse the IMF conditions preceding the detection of the FTEs, which would affect the local conditions in which magnetic reconnection takes place on the dayside magnetopause. As OMNI data provide solar wind conditions at the nose of the bowshock, we estimate the propagation time of the solar wind flow to be approximately 15 min to cross the magnetosheath and reach the magnetopause. The results are not sensitive with intervals between 15 and 30 min.

Figure 4 shows the distribution of the 15-min averaged IMF clock angles ($\theta_{CA} = \arctan(B_y/B_z)$) preceding the events in polar histograms. Panel (a) shows the distribution for RH events and panel (b) shows the distribution for LH events. Positive IMF clock angles ($0° < \theta_{CA} < 180°$) correspond to duskward IMF B_y, while the negative IMF clock angles ($-180° < \theta_{CA} < 0°$) correspond to dawnward IMF B_y. Figure 4 shows that the majority of RH

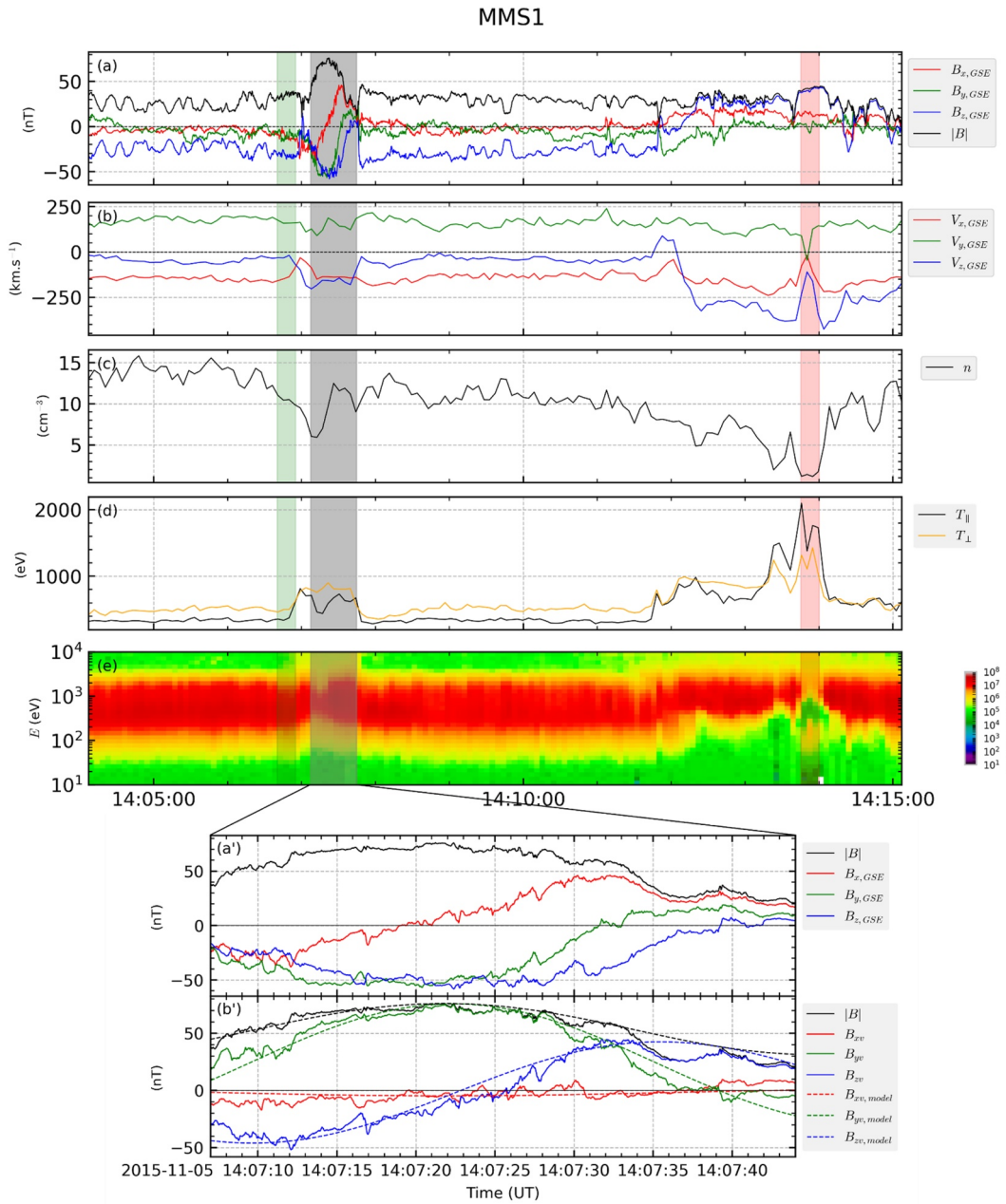

Figure 2. MMS observations of an FTE shown for a 10-min interval (top; panels (a) to (e)) and a 1-min interval (bottom; panels (a') and (b')). The FTE is highlighted in gray in the top panels. Panels (a) show the magnetic field in the GSE coordinate system. Panels (b), (c), (d) show the ion bulk velocity in the GSE coordinate system, the ion number density, and the ion temperature, respectively. Panel (e) shows the ion energy spectogram. The green and red shaded regions mark the adjacent magnetosheath and magnetospheric regions to the FTE, respectively. Panels (a') and (b') show the zoom-in of the panels (a) in GSE and ($\boldsymbol{x}_v$, $\boldsymbol{y}_v$, $\boldsymbol{z}_v$) coordinates system, respectively.

events are preceded by positive IMF clock angles (IMF $B_y > 0$) as seen in panel (a), while the majority of the LH events are preceded by negative IMF clock angles (IMF $B_y < 0$) as seen in panel (b). This group where the FTE helicity sign corresponds to the IMF B_y is referred as the regular group. This group is consistent with a flux rope generation by the multiple X-line reconnection scenario as explained in Kieokaew et al. (2021). However, in Figure 4, there are some events where the helicity sign does not correspond to the IMF B_y for both RH events and LH events. This group, in which we call the "outliers", constitutes 21% of all events. We distinguish the spatial distribution of the outlier group with the red color in Figure 3, while the regular group is presented in blue.

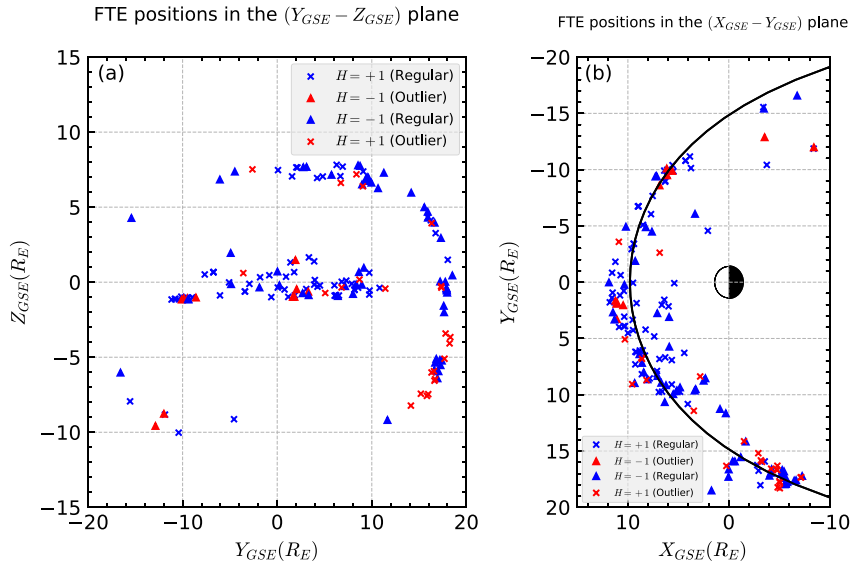

Figure 3. Spatial distribution of the FTEs in the GSE coordinate system in the (a) Y-Z and (b) X-Y planes. The RH ($H = +1$) events are denoted by crosses and the LH ($H = -1$) events are denoted by triangles. We distinguish the outlier events (in red) and regulars (in blue). The solid black line in panel (b) represents the magnetopause boundary from the Shue model with $r_0 = 9.8\ R_E$ and $\alpha_{MP} = 5.6$.

To investigate the solar wind conditions that might control the regular and outlier events, we also investigate other parameters such as the ion bulk velocity, ion number density, Mach number, and ion temperature. We do not find a correlation between those upstream parameters and the flux rope helicity sign. To investigate local effects, we investigate the conditions at the magnetopause where the FTEs may be generated. In particular, we focus on the local magnetic shear properties between the magnetosheath and the magnetospheric magnetic fields in the vicinity of the FTEs.

3.4. Local Magnetic Shear Properties

As there is no clear correlation between the upstream solar wind parameters and the helicity sign of the outlier group, we now shift our focus to investigate local magnetopause properties. We employ two approaches to determine the local magnetic shear. First, we explore the model proposed by Trattner et al. (2007) that estimates the local shear angle across the magnetopause surface by assuming a draping of the IMF and the local flow (Cooling et al., 2001). For a given averaged IMF clock angle for each FTE, we obtain a spatial distribution of the magnetic shear on the magnetopause surface. Figure 5 shows the local, 2-D magnetic shear angle map for a given IMF clock angle at 225.5° (IMF cone angle at 99° and dipole tilt angle at − 8°) on the magnetopause in the (Y_{GSM},

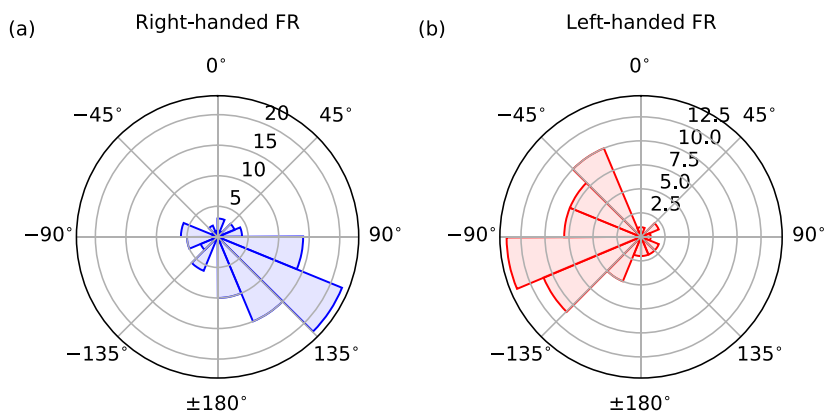

Figure 4. Distribution of the averaged IMF clock angle for (a) RH events, (b) LH events.

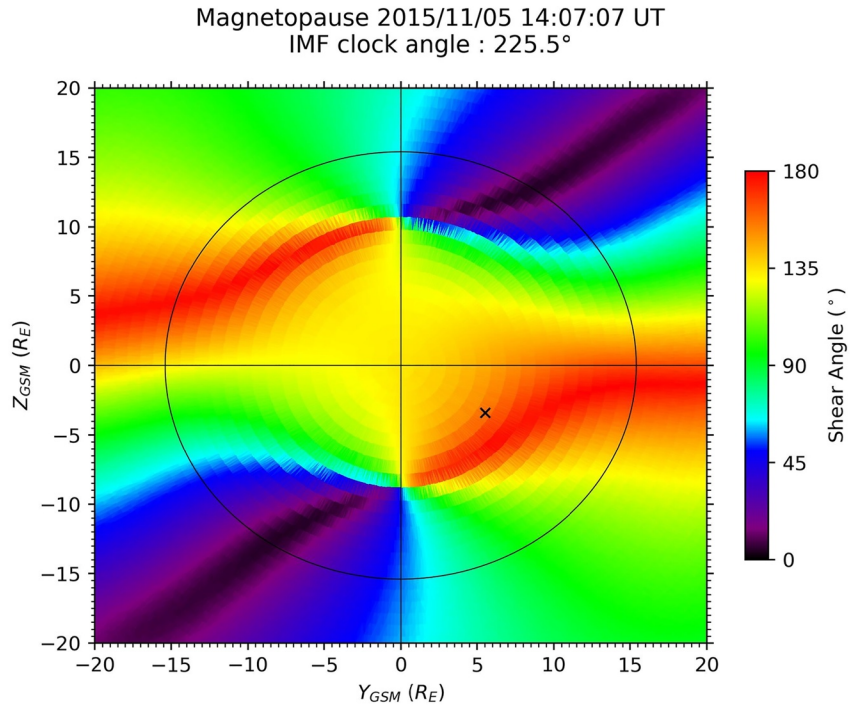

Figure 5. The magnetic shear angle map at the magnetopause surface projected onto the *Y*-*Z* plane of the GSM coordinate system. The map is obtained for the event in Figure 2 on November 5th, 2015 at 14:07:07 UT produced using the averaged IMF clock angle (at 225.5°) preceding the event. The color scale represents the local magnetic shear angle from 0° (dark purple; no shear) to 180° (red; highest shear). The black cross marks the FTE location. The black circle denotes the terminator ($X_{GSM} = 0$).

Z_{GSM}) plane on November 5, 2015, at 14:07:07 UT; the black cross (at $Y = 5.5\ R_E$, $Z = -3.4\ RE$) locates the position of the FTE. This approach allows us to model local magnetic shear at the FTE location, which may indicate the local condition in which the FTE is formed, e.g., by magnetic reconnection near the location of the FTE. Figure 6 shows a histogram of the distribution of the magnetic shear angle modeled at the FTE location for all 166 events. We categorize the data into the regular and outlier groups, represented by solid black and dashed red lines, respectively. We find that the majority of the outlier group has large magnetic shears with the events being mainly around 150°. In contrast, we find that the regular flux ropes have a broader distribution centered around moderate magnetic shear angles.

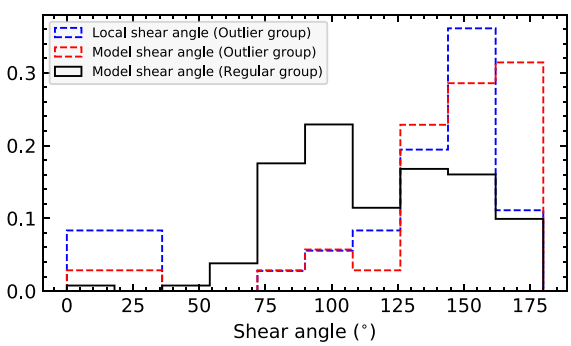

Figure 6. Distributions of the magnetic shear angle associated with the FTEs. The distributions of regular and outlier groups obtained from the model (Trattner et al., 2007) are shown with black solid and red dashed lines, respectively. The distribution of the outlier group obtained from in-situ data is shown in blue dashed line. The distributions are normalized to the total number of each group.

To check whether the magnetic shear angles from the model are consistent with the observed shear properties, we also obtain local shear angles using the data surrounding the outlier flux ropes. The procedure is as follows. We select two regions, one in the magnetosphere and one in the magnetosheath. The magnetosphere has low density but high temperature, while the magnetosheath has a larger density and lower temperature. We avoid strong current layers, regions with jets, accelerated particles or other flux ropes, throughout the selection process. We find that most of the flux ropes are found on the magnetosheath side in the observations. We select a magnetosheath region and a magnetosphere region that are adjacent or close to the studied flux rope. The magnetosphere is generally found from 1-min to 1-hour away from the flux rope (Figure 2). We calculate the shear angle by calculating $\arccos\left(\frac{\boldsymbol{B}_{sp}\cdot\boldsymbol{B}_{sh}}{|\boldsymbol{B}_{sp}||\boldsymbol{B}_{sh}|}\right)$, where $\boldsymbol{B}_{sp}$ is the magnetic field vector in the magnetosphere, and $\boldsymbol{B}_{sh}$ is the magnetic field vector in the magnetosheath. The results are also shown in Figure 6 as denoted by the dashed blue line. The magnetic shear angles obtained from this alternative method are consistent with the results from the modeling.

4. Discussion

We have investigated the helicity sign of 166 quasi force-free FTEs, with 82 from Cluster and 84 from MMS observations. We found that the helicity sign of most events is ordered by the IMF By polarity, and so that positive IMF clock angles correspond to duskward IMF B_y, while negative IMF clock angles ($-180° < \theta_{CA} < 0°$) correspond to dawnward IMF B_y. We also found that 21% of the events have a helicity sign that does not correspond to the expected IMF By polarity. Our findings are consistent with the main results of Kieokaew et al. (2021), where right-handed FTEs are associated with positive IMF B_y and left-handed FTEs are associated with negative IMF B_y. To investigate the local conditions associated with the FTE formation, we analysed the magnetic shear angle using both modeling and in-situ data at the FTE locations. We found that the majority of the outlier FTEs (those whose expected helicity does not correspond to the IMF B_y polarity) are located in generally higher magnetic shear regions.

As a first simple explanation, for a given small IMF B_y the determination of the core field and helicity sign at low guide field (e.g., for high shears) may be more random because of the uncertainties in mapping the IMF observations to the magnetopause (making the helicity - IMF B_y relation less clear at low guide field). In the absence or the presence of a finite low guide field, Karimabadi et al. (1999) demonstrated using hybrid simulations that the Hall magnetic field plays a key role in determining the core field of flux ropes. Similar to their conclusions, we propose that the core field and associated helicity sign of outlier FTEs are explained by the interplay between the Hall and guide fields (e.g., Aunai et al., 2011), during low guide field conditions, rather than just randomness, as explained next.

Our findings in Figure 6 show that the outlier flux ropes (shown in red and in blue) are mostly characterised by high magnetic shears (125°–180°), while the regular flux ropes (shown in black) show a broad distribution with a maximum value around moderate magnetic shears (~100°). This finding suggests that the core field and helicity sign of flux ropes is affected by the local magnetic shear properties in their vicinity. Assuming the magnetic shear at the FTE generation site is not too different from that at their observed locations, we may consider a core field and thus helicity generation mechanism as follows. In the presence of a significant guide field, e.g., at moderate shear angle, the core field and the helicity sign of the generated FTE are likely determined by the guide field of magnetic reconnection (e.g., Karimabadi et al., 1999). Since the IMF B_y is the main component that provides the reconnection guide field under southward IMF conditions, the helicity sign of the produced FTE therefore corresponds to the IMF B_y polarity. This mechanism may explain the regular flux ropes found in our study and in Kieokaew et al. (2021). In the presence of a weak guide field, e.g., at higher magnetic shear, however, the determination of the FTE core field and helicity appears less clear. We now explain in more details how the Hall physics of magnetic reconnection in the absence of guide field may determines the core field and helicity sign of FTE flux ropes.

Near the X-line of anti-parallel magnetic reconnection, i.e., in the ion diffusion region, the Hall electric field is produced as ions meander around the magnetic null while electrons remain frozen-in. Under symmetric inflow conditions, this Hall electric field drags out the newly reconnected magnetic fields and produces a quadrupolar pattern in the out-of-plane (guide field) direction (e.g., Borg et al., 2005; Denton et al., 2016; Mandt et al., 1994; Nagai et al., 2001). At the dayside magnetopause, magnetic reconnection is asymmetric due to the denser plasma in the magnetosheath. Thus, the Hall field pattern on the magnetosheath side dominates and leads to a more bipolar Hall pattern (e.g., Eastwood et al., 2013; Karimabadi et al., 1999; Y. C. Zhang et al., 2017). Since the outlier events are mostly found for high magnetic shears, we expect that their core field, and in turn their helicity, is determined by the Hall field, consistent with previous works by Karimabadi et al. (1999), Teh, Abdullah, and Hasbi (2014) and Teh, Nakamura, et al. (2014).

To summarize the process explained above, Figure 7 shows a schematic of FTE flux rope generation in asymmetric magnetic reconnection under magnetopause-like conditions. Panel (a) shows conditions without a guide field, i.e., anti-parallel reconnection, while panel (b) shows the conditions with a guide field, i.e., component reconnection. The solid black lines denote the projection of magnetic field lines and the dashed black lines denote the separatrices, with black arrows indicating their directions. We mark the plasma inflow with an orange arrow and the plasma outflows with green arrows. The Hall pattern is represented by the circles with crosses or dots on the separatrices indicating the in- and out- of-plane magnetic field directions, respectively. In panel (a), the guide field is absent (or weak), and the Hall magnetic field pattern is more dominant on the magnetosheath side than

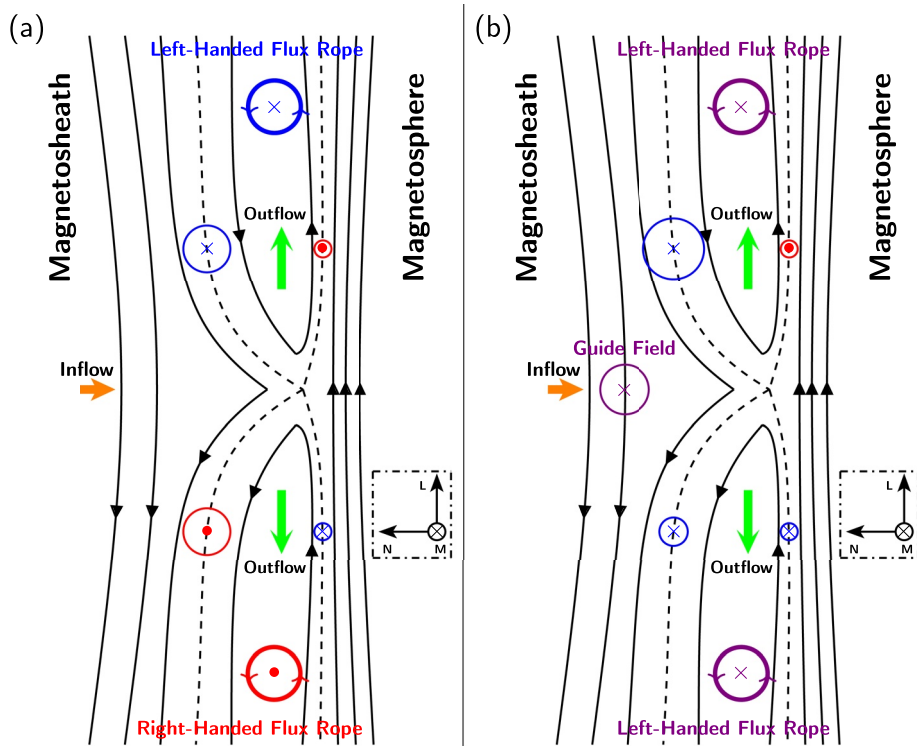

Figure 7. Schematic illustration of (a) anti-parallel and (b) component or guide field magnetic reconnection. Solid black lines represent the magnetic field lines and the dashed black lines represent the separatrices. Blue and red circles represent the Hall pattern, with their sizes corresponding to the magnitude of the Hall field which is stronger in the magnetosheath side due to the asymmetry in the inflow plasma density. In panel (b), the purple circle represents the guide field. The thicker circles represent the flux ropes generated in the reconnection exhausts. Green arrows represent the reconnection outflow, while orange arrows represent the inflow. We note that these illustrations focus on the role of the Hall field at the dominant X-line and thus do not represent the complete FTE helicity generation that involves multiple X-line reconnection (see text).

the magnetospheric side due to the denser plasma (Mozer & Hull, 2010); we denote this dominant Hall field with the bigger circles. In this case, the Hall pattern on the magnetosheath side determines the core field of the flux ropes, and in turn the helicity; they are represented by the thick blue and red circles. In panel (b), however, the presence of a significant guide field reverses the effect of the Hall field and/or, to first order, adds up with it to determine the core field and helicity of the FTEs. They are illustrated with purple circles, e.g., for inward guide field. In brief, these simplified scenarios explain how the FTEs generate their core fields under anti-parallel (high shear) and component (moderate shear) magnetic reconnection (Karimabadi et al., 1999), leading to helicity signs as reported in our study. To further support this scenario, we include results from the simulation previously published by Chen et al. (2020) as outlined next.

The present study corroborates previous work on FTE core field generation as a result of the Hall pattern. While to our knowledge our study is the first statistical analyses of in-situ observations of this process, previous simulations by Karimabadi et al. (1999) originally proposed such a mechanism. Figure 8 shows simulation results from the MHD with embedded particle-in-cell (MHD-EPIC) model with a purely southward IMF condition (no guide field) published by Chen et al. (2020). The color scale shows the out-of-plane magnetic field intensity (B_y component) projected onto the $X-Z$ plane of the GSM system, i.e., as viewed from the dawn side. Panels (a) and (b) show the time evolution of FTE generation due to sequential reconnection X-line formation. The box delineated by a black line represents the region that is simulated using the PIC code to include the kinetic physics of magnetic reconnection. Here, panel (a) shows the first reconnection X-line formation as marked by a red star. The polarity of B_y north and south of the X-line shows negative and positive values, respectively. This bipolar B_y variation is the bipolar Hall pattern produced as a consequence of asymmetric reconnection with the denser plasma in the magnetosheath side. Panel (b) shows the simulation about 7 min later when the first X-line has propagated northward while the second and the third reconnection X-lines sequentially appear as marked with gray stars.

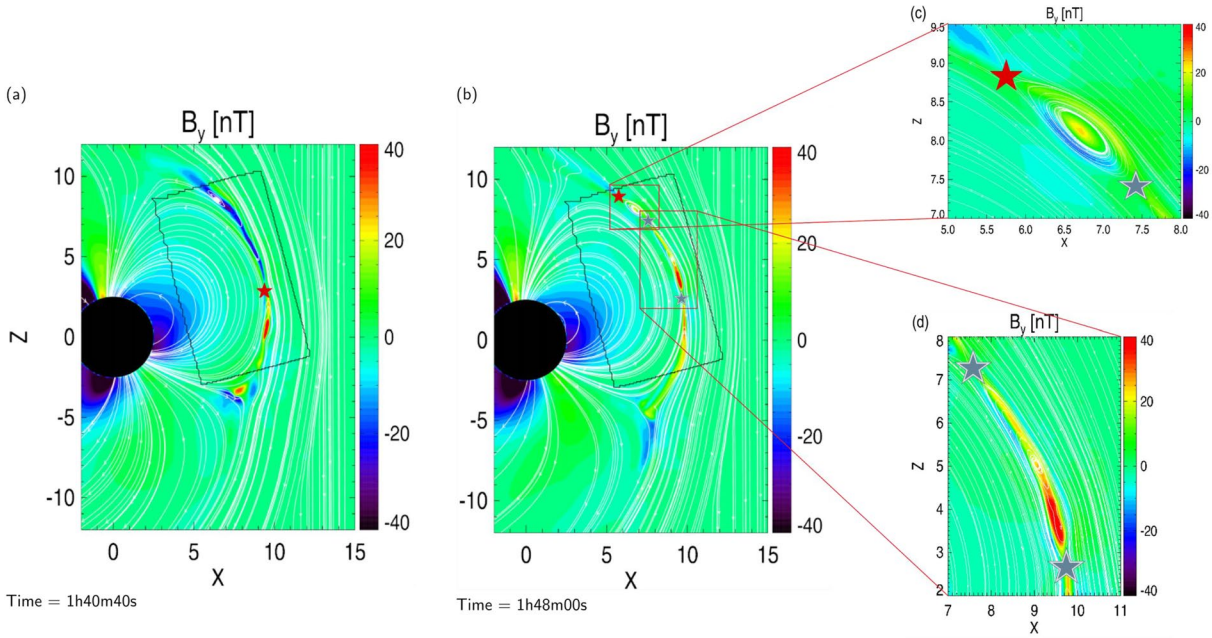

Figure 8. The evolution of the dayside magnetopause using a global MHD simulation embedded with PIC code for the area delineated by a black square. The simulation shows the magnetic field B_y component in the $X-Z$ plane in the GSM coordinate system as viewed from the dawn side. Panel (a) shows a snapshot where a reconnection X-line is first formed as marked by a red star. Panel (b) shows a snapshot around 7 min later of panel (a) where the second and third X-lines, marked by gray stars, are now formed. Panel (c) shows a zoom-in of an FTE formation between the first and the second X-lines. Panel (d) shows a zoom-in of another FTE formation between the second and the third X-lines.

Between the first and second X-lines in panel (b), as zoomed-in in panel (c), an FTE bounded by a white contour forms. The key observation here is that the core field of this FTE retains the Hall pattern of the two X-lines. In other words, panel (c) illustrates an example of how an FTE generates its core field from the Hall magnetic field of magnetic reconnection. Additionally, panel (d) shows a zoom-in of the second and third X-lines. Here, another FTE with the same core field as generated by the initial Hall perturbation is also being formed. Despite the Hall magnetic field perturbation, the formation of the FTEs follows the standard mechanism proposed by Raeder (2006) under large dipole tilt angle, where an FTE can be generated between multiple X-lines. Based on our statistical results and this simulation work, we conclude that the outlier FTE core fields and ensuing helicity are determined from the Hall magnetic field of magnetic reconnection for a weak guide field condition. In brief, the Hall magnetic field leads to the core field and thus the helicity sign of FTEs in the absence of a guide field.

In magnetic reconnection, the Hall field intensity is likely determined by the inflow plasma properties (e.g., Le et al., 2009), and the Hall structure may be controlled by the Alfvén speed profile in asymmetric reconnection (Dai, 2018). The properties of reconnection Hall field may consequently control the core field of FTEs in a low guide field environment, a possibility that deserves to be investigated in the future. In Figure 6, we find that the outlier flux rope becomes dominant over the regular flux rope distribution for magnetic shears higher than about 125°. This behavior suggests that the Hall field starts to dominate over the guide field in determining the final flux rope helicity at about such a value. To first order, assuming a symmetric magnetic field (such that for the same reconnecting field component the guide field is the same on both sides of the reconnecting current sheet), a shear angle of 125° corresponds to a ratio between the guide field and reconnecting field of about 0.5. For lower guide field, the effect of the Hall magnetic field thus becomes statistically dominant. This is an approximation, and depending on local conditions, as well as remote conditions near the initial reconnection site, the exact value of the magnetic shear at which a given effect becomes dominant may vary. Our analysis in Figure 6 also shows a small but non-negligible number of FTEs with small shear angles. It is thus possible that these FTEs have propagated from elsewhere where the local conditions have a higher shear, further showing that the suggestive shear value of ∼125° for separating the effects of the Hall and guide fields is very approximate.

The generation of FTEs by multiple X-lines is not just an assumption in our study (see Figure 1 and Section 1) as it is in fact the only valid paradigm to interpret our results. Indeed, considering the role of the Hall magnetic

field in determining both the core field and helicity sign of flux ropes, under low guide field, the single X-line formation mechanism would always create a left-handed flux rope northward of the reconnection site and a right-handed flux rope southward of the reconnection site, as shown in Figure 7a. If it were the case, this would lead to a systematic north-south dichotomy in left-handed and right-handed flux ropes for the outlier group (which occur for low guide field), while this is not observed in-situ. In particular this trend is not observed in Figure 3 where the red crosses and triangles denote the outlier flux ropes (respectively right- and left-handed). Our findings thus support the idea that FTE flux ropes are produced through a multiple X-line mechanism.

So far our discussion on the role of the Hall magnetic field in determining the core field neglected the fact that we are adopting multiple X-line reconnection as a formation mechanism of FTEs. There should be two distinct Hall patterns that would be present at the two X-lines surrounding the FTE flux rope, and that may affect the internal magnetic structure of the FTE. In other words, the Hall pattern is present in the exhausts of the two X-lines surrounding the FTE flux rope. In a low guide field scenario, one of the two Hall signatures may determine the core field of the FTE flux rope. But this raises the question of which X-line is dominant or which X-line controls the core field and helicity sign of the flux rope. Different parameters could come into play to determine which X-line Hall field become dominant. In particular, the simulation shown in Figure 8 suggests that the initial X-line Hall pattern may be dominant. Indeed, the Hall pattern of the initial X-line (represented by a red star in Figure 8) gives the core field and helicity sign of the FTEs generated later in the simulation, as shown in Figures 8c and 8d. Thus the temporal sequence of X-line formation should play an important role in the determination of the flux rope core field and the helicity sign. Nevertheless, this conclusion comes from only one simulation. More dedicated studies are required to confirm whether this conclusion is general. In particular, one may expect that, in addition to the temporal sequence, the reconnection rate at each X-line may have an impact on which Hall field pattern may eventually dominate the flux rope topology. Moreover, we note that an FTE formation may be a continuous process where dynamical processes such as coalescence, erosion, and division due to active magnetic reconnection can influence FTE structures (e.g., Akhavan-Tafti et al., 2019; 2020). The core field of an FTE may thus be an accumulative effect of multiple reconnection with a varying reconnection rate depending on solar wind conditions, as well as the complex FTE evolution due to ongoing reconnection. All these aspects deserve to be further investigated but they are beyond the scope of our study.

5. Summary and Conclusions

We performed a statistical study of the helicity sign of 166 quasi force-free FTEs, 82 of which were observed by Cluster, and 84 by MMS. We found that the helicity sign of the majority of the events corresponds to the IMF B_y polarity; this population is called the regular group. However, we also found that the helicity sign of a significant number of events (21% of the total events) does not correspond to the IMF B_y polarity; this population is called the outlier group. To better understand the formation of regular and outlier FTEs, we investigated the local properties of the magnetopause surrounding the FTE locations. In particular, we modeled, based on the Maximum Magnetic Shear model by Trattner et al. (2007), the local magnetic shear angle for each FTE. We found that the regular group shows a spread distribution with a maximum value around moderate shear angles. For moderate and low shear angles, the guide field expected at the reconnection sites, where FTEs were formed, would control the core field of FTEs, and thus the helicity sign. This situation is consistent with the fact that the IMF B_y controls the helicity sign of the regular group as the IMF B_y represents the main component that provides the reconnection guide field (Kieokaew et al., 2021). For the outlier group, in addition to the model, we have investigated the shear angle using in-situ data surrounding each outlier FTE. We found that they are observed at higher magnetic shear locations meaning lower guide field closer to the reconnection sites. In this case, it is less clear what controls the core field of the outlier FTEs. In particular, there are higher uncertainties on the IMF mapping and therefore a higher randomness may be expected in the determination of helicity and core field under low guide field at the reconnection site. However, under such conditions, another physical process may be at work. Using hybrid simulations, Karimabadi et al. (1999) originally demonstrated that the Hall effect in the reconnection site may control the core field of FTEs. They also discussed that plasma β and the presence of a pre-existing guide field are two important controlling parameters of the Hall-generated field. Our statistical analyses here are consistent with their results regarding the control of the FTE core field by the Hall field in a low guide-field (i.e., high magnetic shear) environment.

At the magnetopause, anti-parallel magnetic reconnection is typically triggered under asymmetric plasma conditions. In this case, the Hall magnetic field has a strongly skewed quadrupolar pattern, so that the pattern looks mostly bipolar with the Hall field in the two exhausts having opposite out-of-plane orientations (Figure 7). We propose that this bipolar Hall pattern in turn controls the core field of FTE flux ropes, and thus, controls their helicity sign. The effect was shown using the results from a global MHD simulation with embedded PIC code (Chen et al., 2020), reproduced here in Figure 8. Our study also supports the multiple X-line mechanism for the process to produce FTEs as we do not observe any north-south dichotomy for the right-handed and left-handed flux ropes for the outlier group, which occurs for low guide field, while under such conditions a generation mechanism based on a single X-line would suggest such a dichotomy between hemispheres. The presence of two X-lines in the vicinity of FTE flux ropes means the existence of two distinct Hall patterns from the two X-lines surrounding the FTE, but only one of them should dominate and determine the core field and helicity of FTEs. For instance, in the case of Figure 8 we find that the initial X-line is dominant and thus the temporal sequence of X-line formation appears to play an important role in determining the dominant Hall effect on subsequent FTE formation. Future work should look into this temporal sequence of X-line formation, and its contribution in determining the dominant Hall field. Of course, attention should also be given to the reconnection rate which should also come into play, in addition to the temporal sequence. Furthermore, the dynamical, complex FTE evolution due to ongoing reconnection at the surrounding X-lines may influence the FTE structures as they propagate. This work highlights an important aspect of the fundamental interconnection between kinetic scale processes of magnetic reconnection and the macroscale structures of FTEs.

Data Availability Statement

MMS, Cluster and OMNI data are available online at https://lasp.colorado.edu/mms/sdc/public/, https://csa.esac.esa.int/csa-web/ and https://omniweb.gsfc.nasa.gov/, respectively.

Acknowledgments
We are grateful for the referees' comments for their constructive criticisms that help improving our work. Work at IRAP was supported by CNRS, CNES and UPS. Our analysis made use of the tools developped at IRAP by the CDPP (AMDA http://amda.cdpp.eu/, and speasy https://pypi.org/project/speasy/) and by E. Penou (CL, http://clweb.irap.omp.eu/). CDPP, the Centre de Données de la Physique des Plasmas, is supported by CNRS, CNES, Observatoire de Paris and Université Paul Sabatier, Toulouse. YC and PAC were supported by NASA Grant 80NSSC22K0323. GT was supported by NSF Grant 1663800. PAC was supported by NSF Grant 1602769, DoE Grant DE-SC0020294, and NASA Grant 80NSSC19M0146. RCF received funding from STFC Consolidated Grant ST/V000942/1. JB was supported by NASA under Contract No. NNG04EB99C.

References

Akhavan-Tafti, M., Palmroth, M., Slavin, J. A., Battarbee, M., Ganse, U., Grandin, M., & Stawarz, J. E. (2020). Comparative analysis of the vlasiator simulations and mms observations of multiple x-line reconnection and flux transfer events. *Journal of Geophysical Research: Space Physics*, *125*(7), e2019JA027410. https://doi.org/10.1029/2019JA027410

Akhavan-Tafti, M., Slavin, J. A., Sun, W. J., Le, G., & Gershman, D. J. (2019). MMS Observations of Plasma Heating Associated With FTE Growth. *Geophysical Research Letters*, *46*(22), 12654–12664. https://doi.org/10.1029/2019GL084843

Aunai, N., Retinò, A., Belmont, G., Smets, R., Lavraud, B., & Vaivads, A. (2011). The proton pressure tensor as a new proxy of the proton decoupling region in collisionless magnetic reconnection. *Annales Geophysicae*, *29*(9), 1571–1579. https://doi.org/10.5194/angeo-29-1571-2011

Balogh, A., Carr, C. M., Acuña, M. H., Dunlop, M. W., Beek, T. J., Brown, P., et al. (2001). The Cluster Magnetic Field Investigation: Overview of in-flight performance and initial results. *Annales Geophysicae*, *19*, 1207–1217. https://doi.org/10.5194/angeo-19-1207-2001

Berger, M. A. (1982). Rapid reconnection and the conservation of magnetic helicity. *Bulletin of the American Astronomical Society*, *15*.

Berger, M. A. (1984). Magnetic helicity: Gauge-invariant formulation and conservation properties. *Bulletin of the American Astronomical Society*, *16*.

Berger, M. A. (1999). Introduction to magnetic helicity. *Plasma Physics and Controlled Fusion*, *41*(12B), B167–B175. https://doi.org/10.1088/0741-3335/41/12b/312

Berger, M. A., & Field, G. B. (1984). The topological properties of magnetic helicity. *Journal of Fluid Mechanics*, *147*, 133–148. https://doi.org/10.1017/S0022112084002019

Borg, A. L., Øieroset, M., Phan, T. D., Mozer, F. S., Pedersen, A., Mouikis, C., et al. (2005). Cluster encounter of a magnetic reconnection diffusion region in the near-earth magnetotail on september 19, 2003. *Geophysical Research Letters*, *32*(19). https://doi.org/10.1029/2005gl023794

Bothmer, V., & Schwenn, R. (1998). The structure and origin of magnetic clouds in the solar wind. *Annales Geophysicae*, *16*(1), 1–24. https://doi.org/10.1007/s00585-997-0001-x

Burch, J. L., Moore, T. E., Torbert, R. B., & Giles, B. L. (2016). Magnetospheric Multiscale Overview and Science Objectives. *Space Science Reviews*, *199*, 5–21. https://doi.org/10.1007/s11214-015-0164-9

Burlaga, L. F. (1988). Magnetic clouds and force-free fields with constant alpha. *Journal of Geophysical Research*, *93*(A7), 7217–7224. https://doi.org/10.1029/JA093iA07p07217

Chen, Y., Tóth, G., Hietala, H., Vines, S. K., Zou, Y., Nishimura, Y., et al. (2020). Magnetohydrodynamic with embedded particle-in-cell simulation of the geospace environment modeling dayside kinetic processes challenge event. *Earth and Space Science*, *7*(11), e2020EA001331. https://doi.org/10.1029/2020ea001331

Cooling, B. M. A., Owen, C. J., & Schwartz, S. J. (2001). Role of the magnetosheath flow in determining the motion of open flux tubes. *Journal of Geophysical Research*, *106*(A9), 18763–18775. https://doi.org/10.1029/2000ja000455

Cowley, S. W. H. (1982). The causes of convection in the earth's magnetosphere: A review of developments during the ims. *Reviews of Geophysics*, *20*(3), 531–565. https://doi.org/10.1029/rg020i003p00531

Dai, L. (2018). Structures of hall fields in asymmetric magnetic reconnection. *Journal of Geophysical Research: Space Physics*, *123*, 7332–7341. https://doi.org/10.1029/2018ja025251

Dasso, S., Mandrini, C. H., Démoulin, P., & Farrugia, C. J. (2003). Magnetic helicity analysis of an interplanetary twisted flux tube. *Journal of Geophysical Research*, *108*(A10). https://doi.org/10.1029/2003ja009942

Denton, R. E., Sonnerup, B. U., Hasegawa, H., Phan, T. D., Russell, C. T., Strangeway, R. J., et al. (2016). Reconnection guide field and quadrupolar structure observed by mms on 16 october 2015 at 1307 ut. *Journal of Geophysical Research: Space Physics*, *121*(10), 9880–9887. https://doi.org/10.1002/2016ja023323

Dorelli, J. C., & Bhattacharjee, A. (2009). On the generation and topology of flux transfer events. *Journal of Geophysical Research*, *114*(A6). https://doi.org/10.1029/2008ja013410

Eastwood, J. P., Phan, T. D., Fear, R. C., Sibeck, D. G., Angelopoulos, V., Øieroset, M., & Shay, M. A. (2012). Survival of flux transfer event (fte) flux ropes far along the tail magnetopause. *Journal of Geophysical Research*, *117*(A8). https://doi.org/10.1029/2012ja017722

Eastwood, J. P., Phan, T. D., Øieroset, M., Shay, M. A., Malakit, K., Swisdak, M., et al. (2013). Influence of asymmetries and guide fields on the magnetic reconnection diffusion region in collisionless space plasmas. *Plasma Physics and Controlled Fusion*, *55*(12), 124001. https://doi.org/10.1088/0741-3335/55/12/124001

Escoubet, C. P., Fehringer, M., & Goldstein, M. (2001). Introduction the cluster mission. *Annales Geophysicae*, *19*(10/12), 1197–1200. https://doi.org/10.5194/angeo-19-1197-2001

Fargette, N., Lavraud, B., Øieroset, M., Phan, T. D., Toledo-Redondo, S., Kieokaew, R., et al. (2020). On the ubiquity of magnetic reconnection inside flux transfer event-like structures at the earth's magnetopause. *Geophysical Research Letters*, *47*(6), e2019GL086726. https://doi.org/10.1029/2019GL086726

Farrugia, C. J., Chen, L.-J., Torbert, R. B., Southwood, D. J., Cowley, S. W. H., Vrublevskis, A., et al. (2011). crater" flux transfer events: High-road to the x line? *Journal of Geophysical Research*, *116*(A2). https://doi.org/10.1029/2010ja015495

Farrugia, C. J., Rijnbeek, R. P., Saunders, M. A., Southwood, D. J., Rodgers, D. J., Smith, M. F., et al. (1988). A multi-instrument study of flux transfer event structure. *Journal of Geophysical Research*, *93*(A12), 14465–14477. https://doi.org/10.1029/ja093ia12p14465

Fear, R. C., Palmroth, M., & Milan, S. E. (2012). Seasonal and clock angle control of the location of flux transfer event signatures at the magnetopause. *Journal of Geophysical Research*, *117*(A4). https://doi.org/10.1029/2011JA017235

Guo, J., Lu, S., Lu, Q., Lin, Y., Wang, X., Huang, K., et al. (2021). Structure and coalescence of magnetopause flux ropes and their dependence on imf clock angle: Three-dimensional global hybrid simulations. *Journal of Geophysical Research: Space Physics*, *126*(2), e2020JA028670. https://doi.org/10.1029/2020ja028670

Hasegawa, H., Wang, J., Dunlop, M. W., Pu, Z. Y., Zhang, Q. H., Lavraud, B., et al. (2010). Evidence for a flux transfer event generated by multiple x-line reconnection at the magnetopause. *Geophysical Research Letters*, *37*, 1. https://doi.org/10.1029/2010GL044219

Hoilijoki, S., Ganse, U., Sibeck, D. G., Cassak, P. A., Turc, L., Battarbee, M., et al. (2019). Properties of Magnetic Reconnection and FTEs on the Dayside Magnetopause With and Without Positive IMF B x Component During Southward IMF. *Journal of Geophysical Research: Space Physics*, *124*(6), 4037–4048. https://doi.org/10.1029/2019ja026821

Hwang, K.-J., Nishimura, Y., Coster, A. J., Gillies, R. G., Fear, R. C., Fuselier, S. A., et al. (2020). Sequential observations of flux transfer events, poleward-moving auroral forms, and polar cap patches. *Journal of Geophysical Research: Space Physics*, *125*(6), e2019JA027674. https://doi.org/10.1029/2019ja027674

Karimabadi, H., Krauss-Varban, D., Omidi, N., & Vu, H. X. (1999). Magnetic structure of the reconnection layer and core field generation in plasmoids. *Journal of Geophysical Research*, *104*, 12313–12326. https://doi.org/10.1029/1999ja900089

Kieokaew, R., Lavraud, B., Fargette, N., Marchaudon, A., Génot, V., Jacquey, C., et al. (2021). Statistical relationship between interplanetary magnetic field conditions and the helicity sign of flux transfer event flux ropes. *Geophysical Research Letters*, *48*(6), e2020GL091257. https://doi.org/10.1029/2020GL091257

King, J. H., & Papitashvili, N. E. (2005). Solar wind spatial scales in and comparisons of hourly wind and ace plasma and magnetic field data. *Journal of Geophysical Research*, *110*(A2). https://doi.org/10.1029/2004ja010649

LaBelle, J., Treumann, R. A., Haerendel, G., Bauer, O. H., Paschmann, G., Baumjohann, W., et al. (1987). Ampte irm observations of waves associated with flux transfer events in the magnetosphere. *Journal of Geophysical Research*, *92*(A6), 5827–5843. https://doi.org/10.1029/ja092ia06p05827

Le, A., Egedal, J., Daughton, W., Fox, W., & Katz, N. (2009). Equations of state for collisionless guide-field reconnection. *Physical Review Letters*, *102*, 085001. https://doi.org/10.1103/physrevlett.102.085001

Leamon, R. J., Canfield, R. C., Jones, S. L., Lambkin, K., Lundberg, B. J., & Pevtsov, A. A. (2004). Helicity of magnetic clouds and their associated active regions. *Journal of Geophysical Research*, *109*(A5). https://doi.org/10.1029/2003ja010324

Lee, L. C., & Fu, Z. F. (1985). A theory of magnetic flux transfer at the earth's magnetopause. *Geophysical Research Letters*, *12*(2), 105–108. https://doi.org/10.1029/GL012i002p00105

Lepping, R. P., Jones, J. A., & Burlaga, L. F. (1990). Magnetic field structure of interplanetary magnetic clouds at 1 au. *Journal of Geophysical Research*, *95*, 11957. https://doi.org/10.1029/ja095ia08p11957

Lundquist, S. (1950). Magnetohydrostatic fields. *Arkiv För Fyzik*, *2*(35), 361–365.

Mandt, M. E., Denton, R. E., & Drake, J. F. (1994). Transition to whistler mediated magnetic reconnection. *Geophysical Research Letters*, *21*(1), 73–76. https://doi.org/10.1029/93gl03382

Martin, C. J., Arridge, C. S., Badman, S. V., Billett, D. D., & Barratt, C. J. (2020). Modeling non-force-free and deformed flux ropes in titan's ionosphere. *Journal of Geophysical Research: Space Physics*, *125*(4), e2019JA027571. https://doi.org/10.1029/2019ja027571

Mozer, F. S., & Hull, A. (2010). Scaling the energy conversion rate from magnetic field reconnection to different bodies. *Physics of Plasmas*, *17*(10), 102906. https://doi.org/10.1063/1.3504224

Nagai, T., Shinohara, I., Fujimoto, M., Hoshino, M., Saito, Y., Machida, S., & Mukai, T. (2001). Geotail observations of the hall current system: Evidence of magnetic reconnection in the magnetotail. *Journal of Geophysical Research*, *106*(A11), 25929–25949. https://doi.org/10.1029/2001ja900038

Øieroset, M., Phan, T. D., Eastwood, J. P., Fujimoto, M., Daughton, W., Shay, M. A., et al. (2011). Direct evidence for a three-dimensional magnetic flux rope flanked by two active magnetic reconnection x lines at earth's magnetopause. *Physical Review Letters*, *107*, 165007. https://doi.org/10.1103/physrevlett.107.165007

Pal, S. (2022). Uncovering the process that transports magnetic helicity to coronal mass ejection flux ropes. *Advances in Space Research*, *70*(6), 1601–1613. https://doi.org/10.1016/j.asr.2021.11.013

Paschmann, G., Haerendel, G., Papamastorakis, I., Sckopke, N., Bame, S. J., Gosling, J. T., & Russell, C. T. (1982). Plasma and magnetic field characteristics of magnetic flux transfer events. *Journal of Geophysical Research*, *87*(A4), 2159–2168. https://doi.org/10.1029/JA087iA04p02159

Pollock, C., Moore, T., Jacques, A., Burch, J., Gliese, U., Saito, Y., et al. (2016). Fast Plasma Investigation for Magnetospheric Multiscale. *Space Science Reviews*, *199*, 331–406. https://doi.org/10.1007/s11214-016-0245-4

Raeder, J. (2006). Flux transfer events: 1. Generation mechanism for strong southward imf. *Annales Geophysicae*, *24*(1), 381–392. https://doi.org/10.5194/angeo-24-381-2006

Rème, H., Bosqued, J. M., Sauvaud, J. A., Cros, A., Dandouras, J., Aoustin, C., et al. (1997). The Cluster Ion Spectrometry Experiment. *Space Science Reviews*, *78*, 303–350. https://doi.org/10.1023/A:1004929816409

Rijnbeek, R. P., Cowley, S. W. H., Southwood, D. J., & Russell, C. T. (1982). Observations of reverse polarity flux transfer events at the earth's dayside magnetopause. *Nature*, *300*, 23–26. https://doi.org/10.1038/300023a0

Russell, C. T. (1990). Magnetic flux ropes in the ionosphere of venus. In *Physics of magnetic flux ropes* (pp. 413–423). American Geophysical Union (AGU). https://doi.org/10.1029/gm058p0413

Russell, C. T., Anderson, B. J., Baumjohann, W., Bromund, K. R., Dearborn, D., Fischer, D., et al. (2016). The Magnetospheric Multiscale Magnetometers. *Space Science Reviews*, *199*, 189–256. https://doi.org/10.1007/s11214-014-0057-3

Russell, C. T., & Elphic, R. C. (1978). Initial isee magnetometer results: Magnetopause observations. *Space Science Review*, *22*, 681–715. https://doi.org/10.1007/BF00212619

Russell, C. T., & Elphic, R. C. (1979). Isee observations of flux transfer events at the dayside magnetopause. *Geophysical Research Letters*, *6*(1), 33–36. https://doi.org/10.1029/GL006i001p00033

Saunders, M. A., Russell, C. T., & Sckopke, N. (1984). Flux transfer events: Scale size and interior structure. *Geophysical Research Letters*, *11*(2), 131–134. https://doi.org/10.1029/gl011i002p00131

Scholer, M. (1988). Magnetic flux transfer at the magnetopause based on single x line bursty reconnection. *Geophysical Research Letters*, *15*(4), 291–294. https://doi.org/10.1029/gl015i004p00291

Shue, J.-H., Song, P., Russell, C. T., Steinberg, J. T., Chao, J. K., Zastenker, G., et al. (1998). Magnetopause location under extreme solar wind conditions. *Journal of Geophysical Research*, *103*(A8), 17691–17700. https://doi.org/10.1029/98JA01103

Sibeck, D. G., Kuznetsova, M., Angelopoulos, V., Glaßmeier, K.-H., & McFadden, J. P. (2008). Crater ftes: Simulation results and themis observations. *Geophysical Research Letters*, *35*(17). https://doi.org/10.1029/2008gl033568

Song, Y., & Lysak, R. L. (1989). Evaluation of twist helicity of flux transfer event flux tubes. *Journal of Geophysical Research*, *94*(A5), 5273–5281. https://doi.org/10.1029/ja094ia05p05273

Southwood, D., Farrugia, C., & Saunders, M. (1988). What are flux transfer events? *Planetary and Space Science*, *36*(5), 503–508. https://doi.org/10.1016/0032-0633(88)90109-2

Teh, W. L., Abdullah, M., & Hasbi, A. M. (2014a). Evidence for the core field polarity of magnetic flux ropes against the reconnection guide field. *Journal of Geophysical Research: Space Physics*, *119*, 8979–8983. https://doi.org/10.1002/2014JA020509

Teh, W.-L., Nakamura, R., Karimabadi, H., Baumjohann, W., & Zhang, T. L. (2014b). Correlation of core field polarity of magnetotail flux ropes with the imf by: Reconnection guide field dependency. *Journal of Geophysical Research: Space Physics*, *119*(4), 2933–2944. https://doi.org/10.1002/2013ja019454

Trattner, K. J., Mulcock, J. S., Petrinec, S. M., & Fuselier, S. A. (2007). Location of the reconnection line at the magnetopause during southward imf conditions. *Geophysical Research Letters*, *34*(3). https://doi.org/10.1029/2006GL028397

Trenchi, L., Coxon, J. C., Fear, R. C., Eastwood, J. P., Dunlop, M. W., Trattner, K. J., et al. (2019). Signatures of magnetic separatrices at the borders of a crater flux transfer event connected to an active x-line. *Journal of Geophysical Research: Space Physics*, *124*(11), 8600–8616. https://doi.org/10.1029/2018ja026126

Trenchi, L., Marcucci, M. F., Rème, H., Carr, C. M., & Cao, J. B. (2011). Tc-1 observations of a flux rope: Generation by multiple x line reconnection. *Journal of Geophysical Research*, *116*(A5). https://doi.org/10.1029/2010ja015986

Wei, H., Russell, C., Zhang, T., & Dougherty, M. (2010). Comparison study of magnetic flux ropes in the ionospheres of venus, Mars and titan. *Icarus*, *206*(1), 174–181. https://doi.org/10.1016/j.icarus.2009.03.014

Wright, A. N., & Berger, M. A. (1990). The interior structure of reconnected flux tubes in a sheared plasma flow. *Journal of Geophysical Research*, *95*(A6), 8029–8036. https://doi.org/10.1029/ja095ia06p08029

Zhang, H., Kivelson, M. G., Angelopoulos, V., Khurana, K. K., Pu, Z. Y., Walker, R. J., et al. (2012). Generation and properties of in vivo flux transfer events. *Journal of Geophysical Research*, *117*(A5). https://doi.org/10.1029/2011ja017166

Zhang, H., Kivelson, M. G., Khurana, K. K., McFadden, J., Walker, R. J., Angelopoulos, V., et al. (2010). Evidence that crater flux transfer events are initial stages of typical flux transfer events. *Journal of Geophysical Research*, *115*(A8). https://doi.org/10.1029/2009ja015013

Zhang, Y. C., Lavraud, B., Dai, L., Wang, C., Marchaudon, A., Avanov, L., et al. (2017). Quantitative analysis of a hall system in the exhaust of asymmetric magnetic reconnection. *Journal of Geophysical Research: Space Physics*, *122*(5), 5277–5289. https://doi.org/10.1002/2016ja023620